Desalination and Water Treatment
www.deswater.com
doi: 10.5004/dwt.2020.25126

181 (2020) 289–299
March

Dynamic sorption of hexavalent chromium using sustainable low-cost eggshell membrane

Amina Lahmar[a], Zhour Hattab[a,*], Radia Zerdoum[b], Nabila Boutemine[a], Ridha Djellabi[a], Naima Filali[a], Kamel Guerfi[a]

[a]*Laboratory of Water Treatment and Valorization of Industrial Wastes, Department of Chemistry, Faculty of Sciences, Badji-Mokhtar University, B.P.12, Annaba 23000, Algeria, emails: zoumourouda20012000@yahoo.fr (Z. Hattab), anima.lahmar@gmail.com (A. Lahmar), bouteminenabila@gmail.com (N. Boutemine), ridha.djellabi@yahoo.com (R. Djellabi), filali_naima@yahoo.com (N. Filali), k_guerfi@yahoo.fr (K. Guerfi)*
[b]*Science and Technology Laboratory of Water and Environment, Faculty of Science and Technology, Mohammed Cherif Messadia University, Souk Ahras 41000, Algeria, email: environnement2004@yahoo.fr (R. Zerdoum)*

Received 29 May 2019; Accepted 4 November 2019

ABSTRACT

The valorization of agricultural and industrial wastes for water remediation is a great environmental and economic gain. The purpose of this work was the preparation and application of the eggshell membrane (ESM) for the recovery of hexavalent chromium from water in the dynamic adsorption system. To understand the adsorptive behavior of ESM and its surface characteristics, the powder was fully characterized using several techniques such as scanning electron microscopy, Brunauer–Emmett–Teller, Fourier transform infrared spectroscopy, X-ray diffraction, Zeta potential, thermogravimetric analysis, and differential scanning calorimetry. It was found that the ESM is rich with amides, amines, and carboxylic groups and exhibits a porous and interlaced fibrous morphology which is suitable for the fixation of metal ions. The specific surface area was 13.38 $m^2\ g^{-1}$ while the pH_{pzc} of ESM is 7.51. Several operating parameters were investigated such as the bed height, Cr(VI) concentration, pH, ionic strength and temperature. Overall, the best adsorption capacity was found to be 41.49 mg g^{-1} under the following conditions: flow rate of 2 mL min^{-1}, Cr(VI) concentration of 5 mg L^{-1}, bed height of 20 mm, pH 3 and a temperature of 298 K. The regeneration of ESM was studied, wherein, the results showed that the ESM can be reused much time for Cr(VI) removal. The adsorption rate decreased from 57.70% to 44.24% after the tenth adsorption for the removal of Cr(VI) at 10 ppm. Five models were applied including Thomas, Yoon–Nelson, Bohart–Adams, Wolborska, and BDST to model the experimental dynamic adsorption of Cr(VI) on ESM.

Keywords: Egg-shell membrane; Hexavalent chromium; Dynamic adsorption; Regression; Modeling

1. Introduction

Water pollution is reconsidered as one of the biggest environmental issues which we are facing today, due to the dramatic population growth and the large industrial activities, resulting in high discharge of domestic/industrial wastewaters. Heavy metals are one of the major types of pollutants that can be found in a range of industrial wastewater because of the large use of such elements in different industries. Because heavy metals are not biodegradable in the environment, they tend to accumulate in the living organisms which results in different types of diseases that ultimately threaten the life of people. Of these metals, chromium is widely used in different industrial activities

* Corresponding author.

including alloys/metallurgy, textile, electroplating, textile dyeing and leather tanning, which results in large contaminated water with chromium. Cr(VI) is potentially toxic, carcinogenic and mutagenic [1–4]. The tolerance level for chromium Cr(VI) in drinking water is fixed at 0.5 mg L^{-1} according to the World Health Organization [5].

Several techniques have been applied for the removal of heavy metal, including Cr(VI), from water consist usually of chemical/electrochemical precipitation, membrane filtration, adsorption, ion-exchange, coagulation/flocculation and photocatalysis [6–16]. However, these methods exhibit some drawbacks such as low efficiency, the use of large quantities of chemicals and energy. Of these techniques, the adsorption system is very convenient and easy to operate for the removal of heavy metals from water. Since the activated carbon, the most adsorbent used is quite expensive and requires a high cost of regeneration, recently a huge attention has been paid to the valorization and use of effective low-cost agricultural and industrial wastes, and lignocellulosic materials as bioadsorbents for water purification [17–22]. In bio-adsorption, the removal of metal ions species is involved in the physicochemical fixation/binding of such ions onto the surface of the adsorbent which is of bio origin via functional groups. Cationic metal can be fixed by amine groups as chelating agents, while, the electrostatic absorption of anionic metals can occur. Recently, eggshell membrane (ESM) waste has been used widely for the removal of Cr(VI) from water as a biosorbent due to its efficiency and chelating propriety [23–25]. It contains many functional groups in its surface such as amines, amides, and carboxylic groups. Bin and Huang [25] reported that a part of adsorbed Cr(VI) onto the surface of ESM was reduced to less toxic Cr(III) in Cr_2O_3 or $Cr(OH)_3$ during the adsorption process. They suggested that $HCrO_4^-$ firstly is adsorbed on the surface of ESM via the electrostatic interaction with amide groups followed by reduction reaction on the surface ESM, afterward, the Cr(III) is adsorbed/deposited on the surface via chelation or precipitation.

Herein, the removal of Cr(VI) was carried dynamically in a fixed bed column system which contains ESM as an adsorbent. ESM powder was prepared and characterized by different techniques. The effect of some operating parameters was investigated.

2. Materials and methods

ESM was collected from egg waste. Hydrogen chloride (HCl), sodium hydroxide (NaOH), sodium chloride (NaCl), sulphuric acid H_2SO_4, 1,5-diphenylcarbazide and potassium dichromate ($K_2Cr_2O_7$) were purchased from Sigma-Aldrich-Fluka (Saint-Quentin, Fallavier, France).

2.1. Preparation of ESM adsorbent

Eggshell waste was collected from local restaurants. The material was cleaned several times with water and then it was boiled in distilled water for 15 min to remove impurities. Afterward, the eggshell membrane was manually separated from the egg waste and dried for 24 h at room temperature. The material was ground in an electric mill and then sieved using a sieve (Afnor, London, UK). Only particles with diameters between 315 and 500 μm were used for the experimental adsorption tests.

2.2. Characterization of ESM

The morphology of ESM was characterized using scanning electron microscopy (SEM) (JEOL JSM 6390LU, Freising, Germany). Surface functional groups of ESM were checked by Fourier transform infrared analysis (FTIR) using IR^{-1} affinity in combination with a single attenuated total reflectance reflection. The crystal structure of ESM was characterized on X-ray diffraction (XRD) (Rigaku Ultima IV, Neu-Isenburg, Germany) using copper radiation Kα (λ = 1.5460 Å), a generator setting of 40 kV, 40 mA, scanning speed 0.01 min^{-1} and an angle of 2θ between 0 and 70. Zeta potential was carried out with an instrument (Zetasizer 2000, Malvern Co., England) equipped with a microprocessor at a temperature of 21°C and a pH of 6.03. Brunauer–Emmett–Teller (BET) specific surface was performed using (NOVA Quantachrome, Boynton Beach, US), at 77 K. Before analysis, each sample was degassed at 150°C for 1 h in a nitrogen atmosphere. Thermogravimetric analysis (TGA) was carried out using (METTLER TOLEDO, Columbus, Ohio, US) (STARe TGA/DSC 3 + System), at a heating rate of 10°C min^{-1} (30 mL min^{-1}) to 600°C under N_2. Differential scanning calorimetry (DSC) was performed on a METTLER TOLEDO (STARe DSC 3 + System) at a heating rate from 10°C min^{-1} (30 mL min^{-1}) to 500°C under N. The point of zero charge (PZC) value were calculated from the curve representing the pH_f–pH_i values as a function of initial suspension pH of ESM. The value of PZC corresponds to the intersection value with the abscissa axis where ΔpH = 0 [26].

2.3. Column adsorption experiments

Adsorption was carried out in a glass column (diameter: 11 mm, length: 300 mm). The residual Cr(VI) concentration was determined at a wavelength of λ_{max} = 545 nm using a UV-Vis spectrophotometer (JENWAY 7315, Staffordshire, England) after complexation with 1,5-diphenylcarbazide [27].

2.4. Analysis of experimental data

Breakthrough curves profiles of Cr(VI) adsorption were obtained from $C_t/C_0 = f(t)$, where C_t and C_0 are effluent and initial concentrations, respectively, t is service time.

The set of equations used in this work are summarized in Table 1 [28].

2.5. Models and kinetic tests of fixed-bed column adsorption

Five theoretical models were applied in this study, the set of equations used in this work are summarized in Table 2: (i) Thomas, it can be used where external and internal diffusion limitations are absent [29]. (ii) Yoon–Nelson, it is based on the hypothesis that the rate of decrease in the probability of the adsorbate molecule is proportional to the probability of penetration of the adsorbate on the adsorbent [30]. (iii) Bohart–Adams describes the initial part of the breakthrough curve [31]. (iv) Wolborska is based on the general mass transfer equations for the scattering mechanism in the range of the low concentration breakthrough curve which can be

Table 1
Table of equations used for fixed-bed analyses

Volume of treated effluent	$V_{\text{eff}} = F\left(t_e\right)$	(1)
Total amount of Cr(VI) adsorbed	$Q_{\text{total}} = \frac{F}{1000} A = \frac{F}{1000}\int_{t}^{t=\text{total}} C_{\text{ads}}\,dt$	(2)
Experimental absorption amount	$Q_{\text{exp}} = \frac{Q_{\text{total}}}{m}$	(3)
Maximum adsorption capacity	$N_{\text{exp}} = Q_{\text{exp}} \frac{m}{V}$	(4)
Quantities of adsorbate passed in the column	$W_{\text{total}} = \frac{C_0 Q t_{\text{total}}}{1{,}000}$	(5)
Percentage of removal	$R\% = \frac{Q_{\text{total}}}{W_{\text{total}}} \times 100$	(6)

applied to experimental data for describing the initial part of the breakthrough curve [32]. (v) BDST, proposed by Bohart and Adams [31] and it is based on the assumption that the adsorption rate is controlled by the surface reaction between the adsorbate and the unused capacity of the adsorbent, it is employed usually to estimate the bed depth required for a given service time [33].

3. Results and discussion

3.1. Characterization of ESM

3.1.1. SEM analysis

SEM images of the ESM sample are shown in Fig. 1. It can be seen the ESM exhibits an interlaced fibrous structure (compact network like with smooth protein fibers) [34]. This porous structure could be suitable for the retention of pollutants.

3.1.2. FTIR analysis

Fig. 2 shows the FTIR spectrum for ESM. Different peaks were detected which are attributed to various functional groups and bands.

The band at 3,366 cm^{-1} is assigned to N–H and –OH. Bands at 3,070; 2,927 and 2,858 cm^{-1} are attributed to C–H present in =C–H and $=CH_2$. The peak at 1,630 cm^{-1} is due to C=O amide stretching. The absorption peak appearing at around 1,525 cm^{-1} is attributed to N–H amide bonding. Bands at 1,450; 1,190; and 610 $cm^{-1}$are due to CH_2 scissoring, C–N amine stretching and C–S, respectively [35].

3.1.3. X-ray diffraction

The X-ray diffraction spectrum of ESM shown in Fig. 3 indicates that ESM is an amorphous material [36]. Furthermore, a large peak at 2θ, 22° was detected which is assigned to the amides, amines and carboxylic groups in ESM.

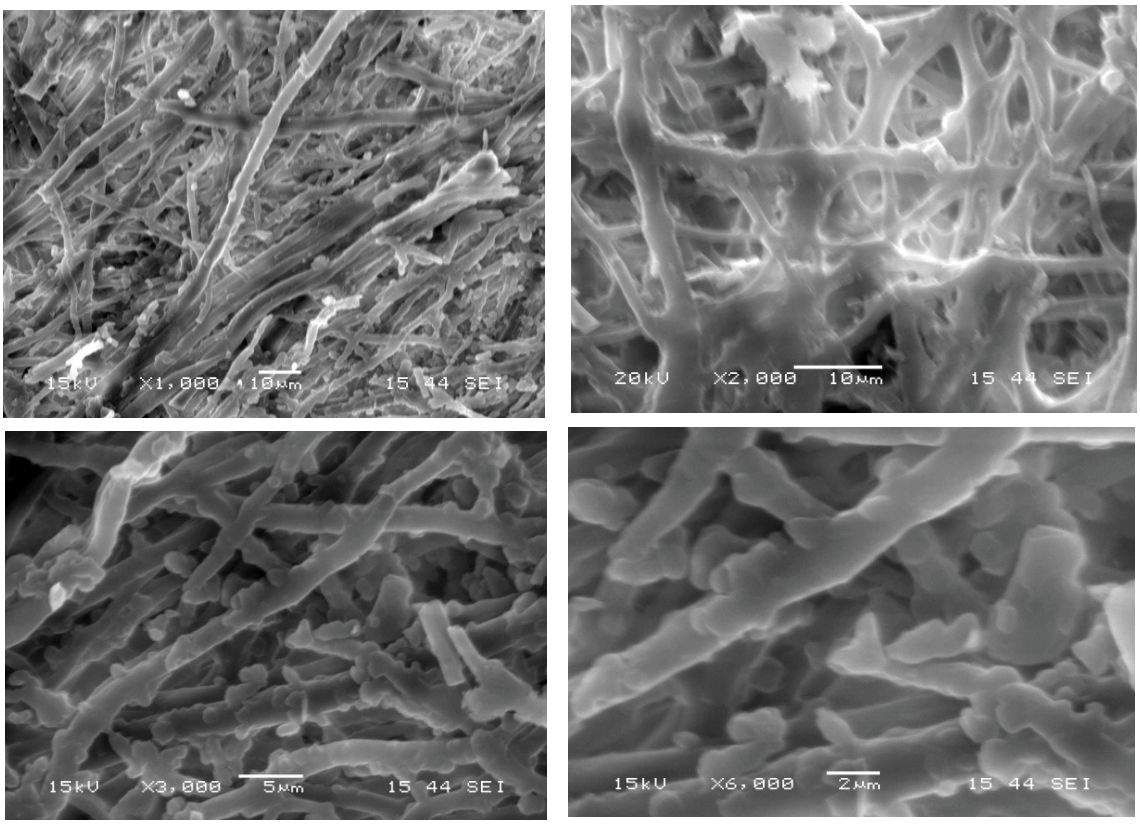

Fig. 1. SEM images of the ESM sample.

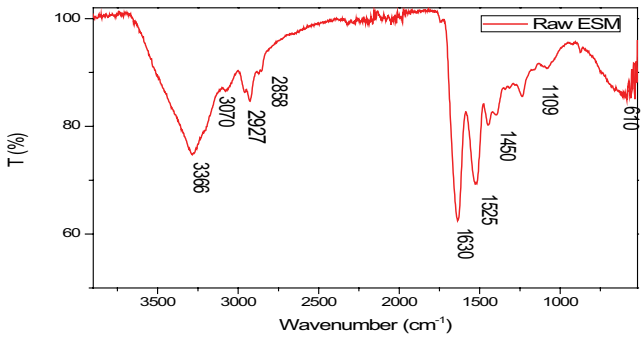

Fig. 2. FTIR spectra of ESM before Cr(VI) adsorption.

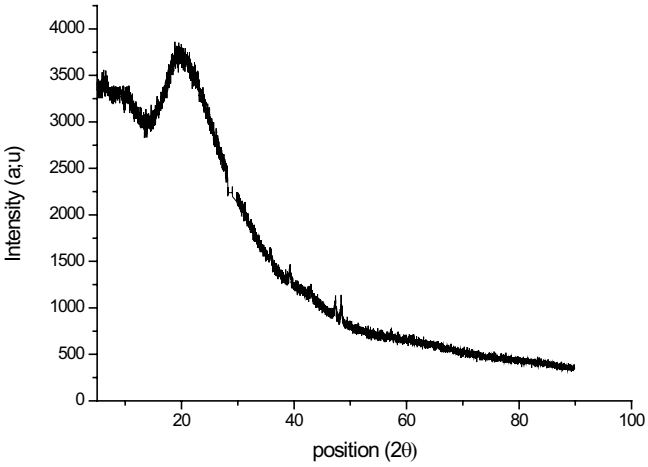

Fig. 3. XRD spectrum of ESM before adsorption.

3.1.4. Zeta potential and BET analysis

The results showed that the zeta potential of ESM was found to be 2.30 (mV), while the particle density was 68.880 g cm^{-3}. The zeta potential measurement reflects the electrical potential at the interface between ESM particles and adjacent liquid. The membrane surface carries positively charged sites produced by basic lateral chains of amino acids. It possesses a surface with special functional groups such as hydroxyl (–OH), amino (–NH_2), carboxyl (–COOH), amide (–$CONH_2$), thiol (–SH), etc. Due to the presence of various functional groups, ESM can be used as a potential adsorbent [37].

Table 3 depicts the results of the BET specific surface area. ESM exhibits a surface area of 13.38 m^2 g^{-1} and a pore diameter of 22.13 (Å) (mesoporous type according to International Union of Pure and Applied Chemistry (IUPAC)) [38].

3.1.5. TGA analysis

TGA of ESM is shown in Fig. 4. Three phases of weight loss are distinct in the curve. The first phase 25°C–120°C corresponds to a rapid loss of about 6.92%of the sample weight (dehydration) due to water molecules held at the surface by hydrogen bonding [39]. The second weight loss is 50.38% in the temperature range of 220°C–400°C. This could contribute to the degradation of collagen and glycane chains, the

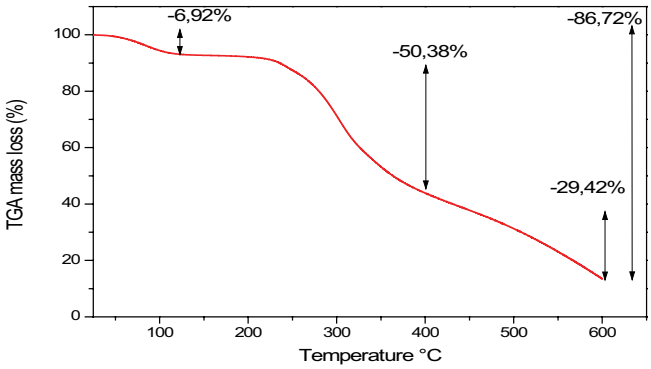

Fig. 4. TGA analysis of ESM.

third phase 400°C–600°C is that of membrane degradation 29.42% [35].

3.1.6. DSC analysis

The DSC is represented in Fig. 5 which shows an endothermic heat peak at 120°C probably due to the loss of moisture and residual protein [40]. It can be noted that the inflammation temperature is 200°C. The degradation of collagen chains, glycane chains and membrane takes place at 220°C–300°C, 300°C–400°C and 400°C–500°C, respectively. These results are in agreement with the results of TGA.

3.1.7. Point of zero charge (PZC)

Fig. 6 shows that the ESM's pH_{pzc} is equal to 7.51, which implies that its surface is negatively charged at pH > 7.51 and positively charged at pH < 7.51.

3.2. Effect of flow rate

Different flow rates of 1, 2 and 3 mL min^{-1} were tested using a peristaltic pump (ISMATEC A39494, Wertheim, Germany) to adsorb Cr(VI) by ESM. According to Fig. 7 and Tables 2 & 4, the increase of flow rate reduces the operating times and results in a decrease in the adsorption capacity. This behavior can be explained by the insufficient contact time for mass transfer between the adsorbate and ESM biomass, diffusion of solute into the pores of the biosorbent and a limited number of active sites and ionic biomass groups for matrix biosorption [41].

3.3. Effect of bed height

Different quantities of ESM, 0.06, 0.12 and 0.18 g corresponding to bed heights of 10, 20 and 30 mm, respectively, were used.

When the mass of sorbent forming homogeneous fixed bed, which is proportional to the height of the bed, increases, the number of sorption sites increases, therefore it increases the penetration and exhaustion times and sorption capacity (Fig. 8 and Tables 2 & 4) [42].

3.4. Effect of initial concentration

The adsorption of Cr(VI) at concentrations of 5, 10 and 15 ppm was carried out and the results are shown in

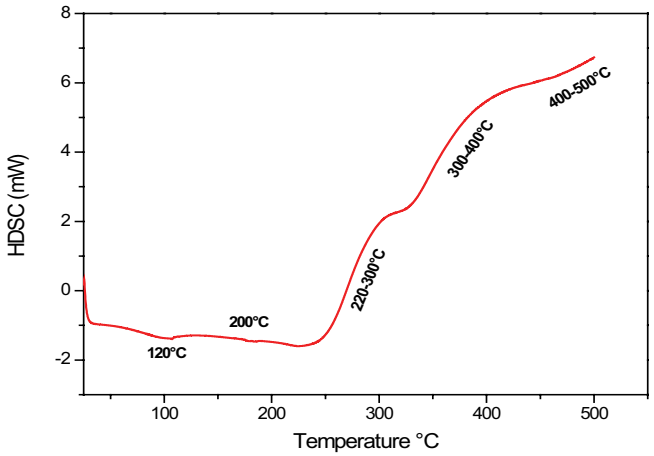

Fig. 5. DSC analysis of ESM.

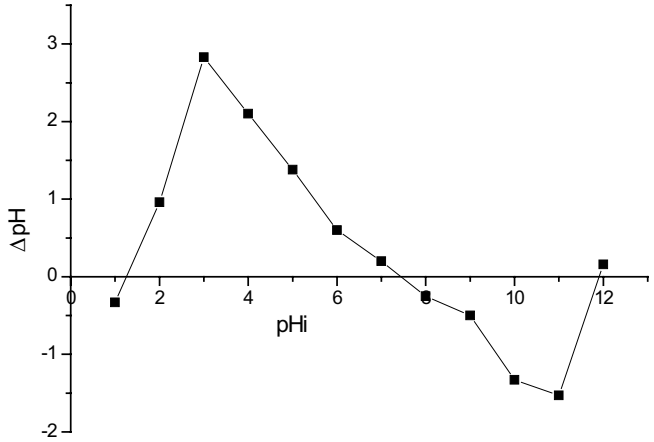

Fig. 6. Point of zero charge of ESM.

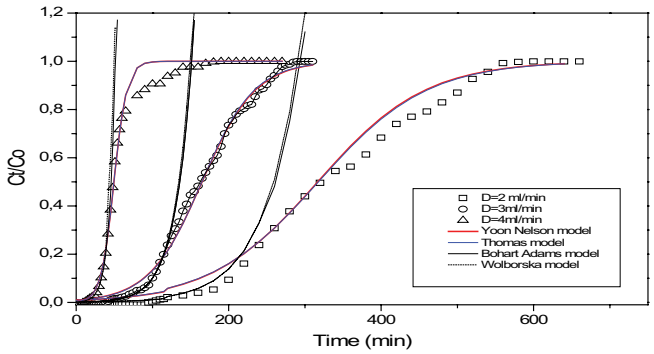

Fig. 7. Comparison of theoretical and experimental penetration curves at different flow rates according to the models studied for Cr(VI) adsorption by ESM (Z = 20 mm, C_0 = 10 mg L^{-1}, pH = 3 ± 0.1, and T = 298 K).

Fig. 9. The removal rates were found to be 88.91%, 57.7%, and 45.42% for Cr(VI) concentration of 5, 10 and 15 ppm, respectively. While, the adsorption capacity values were 41.49, 27.89, 20.44 for Cr(VI) concentration of 5, 10 and 15 ppm, respectively.

Table 2
Five models used for fixed-bed analyses

Model of Thomas	$\frac{C_t}{C_0}=\frac{1}{1+\exp\left(\frac{K_{th}mQ}{U}-C_0K_{th}t\right)}$	(7)
Model of Yoon–Nelson	$\frac{C_t}{C_0}=\frac{1}{1+e^{\mathrm{Kyn}(\tau-t)}}$	(8)
Model of Bohart–Adams	$\frac{C_t}{C_0}=\exp\left(K_{BA}C_0t-K_{BA}N_0\frac{Z}{U}\right)$	(9)
Model of Wolborska	$\frac{C_t}{C_0}=\exp\left(\frac{\beta_aC_0}{N_0}t-\frac{\beta_aZ}{U}\right)$	(10)
Model of BDST	$t_b=\frac{N_0'}{C_0U}Z-\frac{1}{K_{BA}C_0}\ln\left(\frac{C_0}{C_b}-1\right)$	(11)

The adsorbent slowly attains saturation at low concentrations of influents; a low concentration gradient leads to slow down the transport of species due to the reduced diffusion rate [43–46]. As the concentration of Cr(VI) is higher, the breakthrough is steeper [47]. In addition, a decrease in the percentage of adsorption with a higher concentration of adsorbate indicates that the adsorption is dependent upon the availability of the binding sites [48] and it may be due to competition of the Cr(VI) ions for the sites available [49]. The quantity of ESM was fixed, the available sites for adsorption remained constant and a limited amount of Cr(VI) particles decreased the duration of reductive reaction, which then led to low removal efficiency under a high Cr(VI) concentration [49].

3.5. Effect of pH

The effect of pH of the solution on the adsorption of Cr(VI) was studied in the range of 2–4. The results are shown in Fig. 10 and listed in Tables 3 and 4.

It was found that the adsorption capacity is more pronounced at pH = 3, this is explained by the charge on the surface of the adsorbent and the charge of the pollutant studied (attraction-repulsion between adsorbate–adsorbent) [50]. As a function of pH, Cr(VI) can be found in different ionic forms in water such as $H_2Cr_2O_7$ at pH < 1, $HCrO_4^-$ at 1 < pH < 6 and CrO_4^{-2} at pH > 6. Among these anions, the $HCrO_4^-$ is the predominant species of Cr(VI) at pH = 3 [51], therefore, an increase of electrostatic attraction is obtained between $HCrO_4^-$ species and the positively charged surface of ESM at pH < 7.51 according to results of PZC diagram (Fig. 6).

3.6. Effect of ionic strength

It is essential to study the competitive influence of coexisting NaCl ions during Cr(VI) adsorption. As shown in Fig. 11 and Tables 2 & 4, the Cl^- coexisting ions have a significant competitive influence on the adsorption of Cr(VI) which considerably reduces the removal efficiency of Cr(VI).

Cl^- consumes surface sites of adsorbent and thus reduces the available adsorption surface sites for Cr(VI). During this time, the occupied sites decrease the surface charge and thus increase the electrostatic repulsion between surface and anions ($HCrO_4^-$). A similar tendency has been reported by Wang et al [52].

3.7. Effect of temperature

According to Tables 2 and 4, the exhaustion time is reduced at high temperatures, this observation can be explained by the fact that a high functioning temperature favors the diffusion of Cr(VI) molecules in the adsorbent, which permits a short passage time and a rapid saturation of the bed [53], and according to Fig. 12, the efficiency rate and adsorption capacity of Cr(VI) decrease at higher temperatures. This may be due to the failure of some active and internal bonds in sorbent surface sites [24]. Therefore, the adsorption of Cr(VI) on ESM bed was favorized at low temperature, indicating an exothermic process.

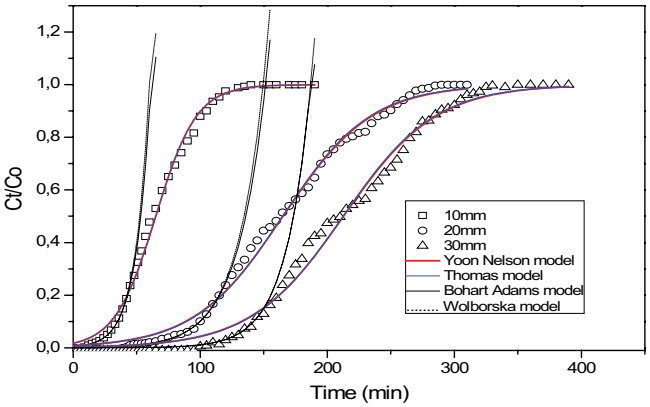

Fig. 8. Comparison of theoretical and experimental penetration curves at different bed height according to the models studied for Cr(VI) adsorption by ESM (F = 2 mL min^{-1}, C_0 = 10 mg L^{-1}, pH = 3 ± 0.1, and T = 298 K).

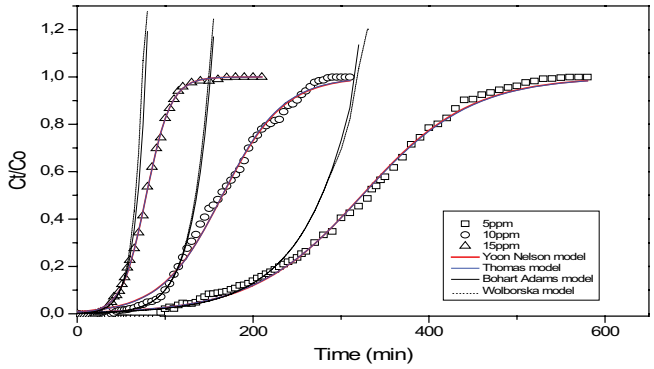

Fig. 9. Comparison of theoretical and experimental penetration curves at different Cr(VI) concentrations according to the models studied for Cr(VI) adsorption by ESM (F = 2 mL min^{-1}, Z = 20 mm, pH = 3 ± 0.1, and T = 298 K).

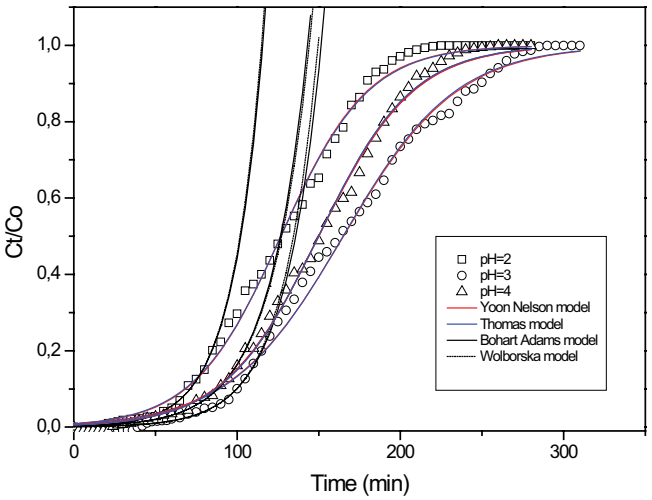

Fig. 10. Comparison of theoretical and experimental penetration curves at different pH according to the models studied for Cr(VI) adsorption by ESM (F = 2 mL min^{-1}, Z = 20 mm, C_0 = 10 mg L^{-1}, and T = 298 K).

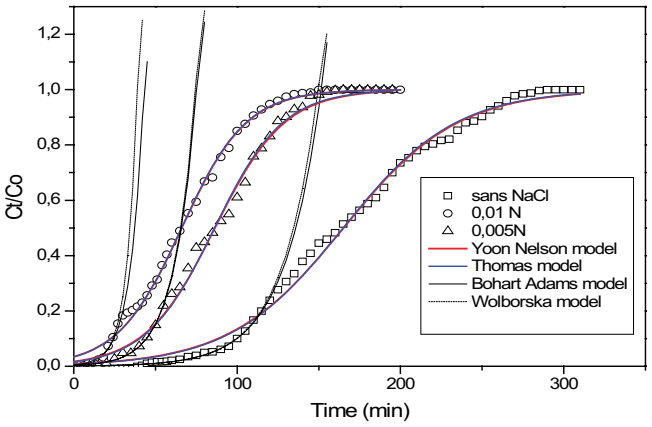

Fig. 11. Comparison of theoretical and experimental penetration curves at different pH concentrations according to the models studied for Cr(VI) adsorption by ESM (F = 2 mL min^{-1}, Z = 20 mm, C_0 = 10 mg L^{-1}, pH = 3 ± 0.1, and T = 298 K).

Table 3
Pore properties of eggshell membrane

Parameters	Specific surface area (m^2 g^{-1})	Total pore volume (cm^3 g^{-1})	Pore diameter (Å)	Particle density (g cm^{-3})
	13.38	0.0138	22.13	0.25

Table 4
Conditions and results for fixed-column Cr(VI) adsorption experiments

C_0 (mg L^{-1})	Z (mm)	F (mL min^{-1})	pH	T (k)	NaCl (N)	t_b (min)	t_{total} (min)	V_{eff} (mL)	W_{total} (mg)	q_{total} (mg)	q_{exp} (mg g^{-1})	R (%)
10	10	2	3	298	0	36	110	220	7.80	1.37	22.88	17.60
10	20	2	3	298	0	100	250	500	5.80	3.34	27.89	57.70
10	30	2	3	298	0	145	290	580	7.00	5.88	32.66	84.01
5	20	2	3	298	0	235	450	900	5.60	4.98	41.49	88.91
15	20	2	3	298	0	42	110	220	5.40	2.45	20.44	45.42
10	20	1	3	298	0	210	520	520	6.00	3.50	29.17	58.34
10	20	3	3	298	0	33	100	300	5.70	1.78	14.88	31.32
10	20	2	4	298	0	35	260	520	5.40	3.00	25.02	55.61
10	20	2	2	298	0	21	225	450	4.70	2.54	21.24	54.23
10	20	2	3	318	0	93	170	340	5.00	2.67	22.33	53.59
10	20	2	3	308	0	97	200	400	5.60	3.05	25.43	54.49
10	20	2	3	298	0.01	24	110	220	3.1	1.37	11.48	44.47
10	20	2	3	298	0.005	45	130	260	3.30	1.77	14.78	53.77

4. Regeneration

The desorption of Cr(VI) species adsorbed onto the ESM bed column was realized by washing with distilled water. The regenerated ESM bed column was reused to adsorb Cr(VI). As can be seen in Figs. 13 and 14, the ESM showed a good performance in removing Cr(VI) from the solution during the ninth adsorption–desorption cycles. It was found that the adsorption capacity for Cr(VI) was reduced after each cycle. The decrease in removal efficiency can be attributed to the loss of partial reduction property of ESM during adsorption–desorption processes. The adsorption efficiency decreased from 57.70% to 44.24% after the tenth adsorption [54].

5. Modeling

5.1. Model of Thomas and Yoon–Nelson

According to Table 5, it is interesting to observe that the R^2 coefficient values for the two models Thomas and Yoon–Nelson are greater than 0.98 for all parameters, also

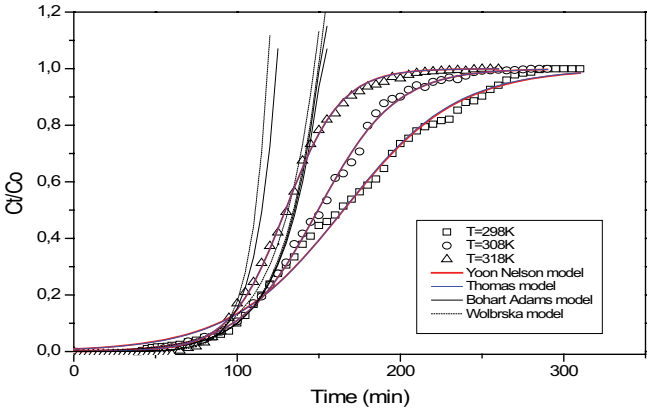

Fig. 12. Comparison of theoretical and experimental penetration curves at different temperature according to the models studied for Cr(VI) adsorption by ESM (F = 2 mL min^{-1}, Z = 20 mm, C_0 = 10 mg L^{-1}, and pH = 3 ± 0.1).

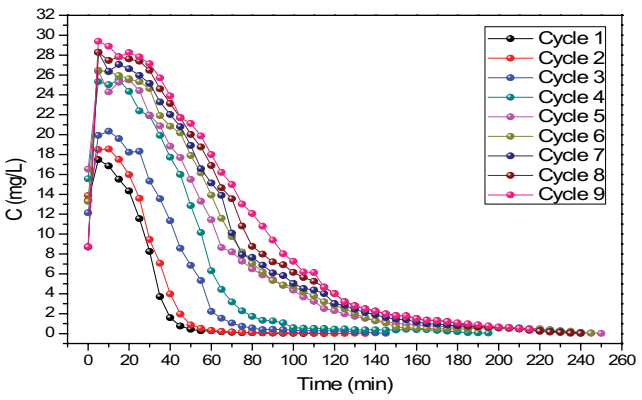

Fig. 13. Desorption of Cr(VI) from ESM column using distilled water (F = 2 mL min^{-1}, Z = 20 mm, C_0 = 10 mg L^{-1}, and T = 298°C ± 1°C).

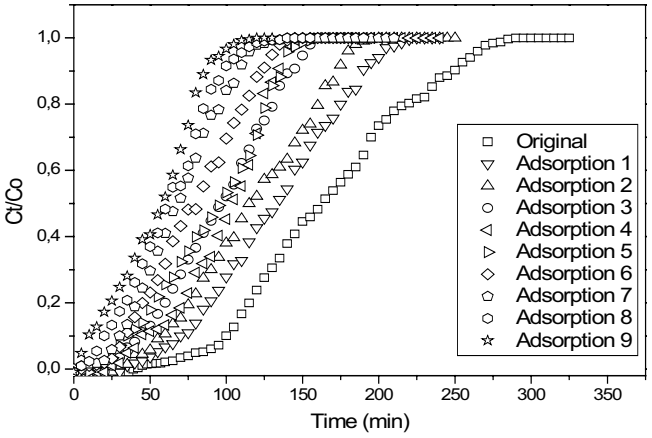

Fig. 14. Breakthrough curves for regenerated ESM (F = 2 mL min^{-1}, Z = 20 mm, C_0 = 10 mg L^{-1}, and T = 298°C ± 1°C).

Table 5
Parameters of Thomas and Yoon–Nelson models for Cr(VI) adsorption by ESM at different conditions using non-linear regression

						Thomas model				Yoon–Nelson model			
C_0 (mg L^{-1})	Z (mm)	F (mL min^{-1})	pH	T (k)	NaCl (N)	$K_{th} \times 10^3$ (ml mg^{-1} min^{-1})	q_{th} (mg g^{-1})	q_{exp} (mg g^{-1})	R^2	$K_{YN} \times 10^3$ (ml min^{-1})	τ (min)	τ_{exp} (min)	R^2
10	10	2	3	298	0	6.22	21.64	22.88	0.9959	62.05	64.95	65	0.9923
10	20	2	3	298	0	2.90	27.48	27.89	0.9958	28.62	165.14	165	0.9939
10	30	2	3	298	0	2.77	23.61	32.66	0.9935	27.37	212.77	215	0.9905
5	20	2	3	298	0	3.23	26.97	41.49	0.9963	15.98	324.13	330	0.9947
15	20	2	3	298	0	4.82	19.66	20.44	0.9993	72.39	78.63	80	0.9987
10	20	1	3	298	0	1.42	28.09	29.17	0.9930	14.02	337.76	335	0.9889
10	20	3	3	298	0	11.78	12.39	14.88	0.9915	117.79	49.57	51	0.9844
10	20	2	4	298	0	3.49	24.97	25.02	0.9976	34.40	149.96	150	0.9972
10	20	2	2	298	0	3.77	21.12	21.24	0.9971	37.23	126.82	125	0.9959
10	20	2	3	318	0	5.88	21.59	22.33	0.9989	59.06	129.53	130	0.9981
10	20	2	3	308	0	4.23	24.91	25.43	0.9987	42.28	149.49	150	0.9979
10	20	2	3	298	0.01	5.08	11.00	11.48	0.9966	50.51	66.10	65	0.9934
10	20	2	3	298	0.005	4.80	14.36	14.78	0.9952	46.99	86.39	85	0.9924

the adsorption capacities and τ values calculated by the two models and the value obtained experimentally are close enough. The rate constant of Thomas and Yoon–Nelson increases with increasing flow rate, however τ decreases accordingly. This is due to the driving force of adsorption [41] and on the fact that a higher flow rate would permit an early achievement of the adsorption equilibrium. It can be argued that both models studied are appropriate to describe Cr(VI) adsorption [55].

5.2. Model of Bohart–Adams and Wolborska

For both models, according to Table 6, the correlation coefficient is greater than 0.90 for all the parameters studied, reflecting the applicability of these two models. Due to the predominance of external mass transfer activities, the mass transfer coefficient increases with increasing flow rate [56].

5.3. Model of BDST

According to Fig. 15 and Tables 5 & 7, all R^2 determination coefficients exceeded 0.98, indicating that the BDST model perfectly represents Cr(VI) adsorption. At C_b/C_0 about 0.7 and 0.9, the constant K_{AB} has negative abnormal values, indicating a certain limitation of the BDST model [57].

6. Conclusion

In this work, ESM was valorized and used as an adsorbent for the removal of Cr(VI) from water in a dynamic system.

Table 6
Parameters of Bohart–Adams and Wolborska models for Cr(VI) adsorption by ESM at different conditions using non-linear regression

						Bohart–Adams model				Wolborska model			
C_0 (mg L^{-1})	Z (mm)	F (mL min^{-1})	pH	T (k)	NaCl (N)	$K_{BA} \times 10^3$ (ml mg^{-1} min^{-1})	N_0 (mg L^{-1})	N_{exp} (mg L^{-1})	R^2	β_a (min^{-1})	N_0 (mg L^{-1})	N_{exp} (mg L^{-1})	R^2
10	10	2	3	298	0	8.80	1,557.78	1,598.85	0.9915	14.05	1,526.76	1,598.85	0.9851
10	20	2	3	298	0	4.46	1,929.86	1,948.95	0.9818	8.80	1,905.13	1,948.95	0.9744
10	30	2	3	298	0	5.16	2,380.29	2,249.62	0.9901	12.28	2,380.29	2,249.62	0.9901
5	20	2	3	298	0	3.47	2,025.63	2,899.32	0.9033	7.02	2,025.11	2,899.32	0.9033
15	20	2	3	298	0	5.35	1,486.90	1,428.34	0.9815	8.53	1,418.71	1,428.34	0.9707
10	20	1	3	298	0	2.18	1,979.56	2,038.39	0.9667	4.32	1,979.51	2,038.39	0.9664
10	20	3	3	298	0	12.68	981.52	1,039.81	0.9903	12.95	956.29	1,039.81	0.9836
10	20	2	4	298	0	4.18	1,824.20	1,723.37	0.9821	7.56	1,837.23	1,723.37	0.9677
10	20	2	2	298	0	5.19	1,474.45	1,463.01	0.9821	7.70	1,465.46	1,463.01	0.9706
10	20	2	3	318	0	7.78	1,581.20	1,560.42	0.9640	13.98	1,513.37	1,560.42	0.9572
10	20	2	3	308	0	4.63	1,913.22	1,777.04	0.9702	8.18	1,874.35	1,777.04	0.9575
10	20	2	3	298	0.01	12.54	546.49	802.22	0.9673	7.66	495.79	802.22	0.9799
10	20	2	3	298	0.005	7.54	957.01	1,032.82	0.9852	7.29	949.06	1,032.82	0.9606

Table 7
Calculated constants of BDST model for Cr(VI) adsorption

C_b/C_0	a (min cm^{-1})	b (min)	$K_{AB} \times 10^3$ (L mg^{-1} min^{-1})	N'_0 (mg L^{-1})	R^2
0.1	5.70	–18.66	11.77	1,452.189	0.9950
0.3	6.00	–3.33	101.11	1,528.62	0.9976
0.5	7.50	–1.66	234.44	1,910.77	0.9941
0.7	8.75	3.33	–127.15	2,229.23	0.9868
0.9	9.00	36.66	–12.24	2,292.93	0.9838

Table 8
Comparison of Cr(VI) adsorption performances by ESM adsorbents

Adsorbent	Adsorption mode	Bed	Amount of adsorbent (g)	Removal of Cr(VI) (%)	References
ESM	Batch		0.05	47	[25]
			3.78	81.47	[51]
	Dynamic		0.5	100	[23]
		2.2 cm × 3 cm	/	100	[23]
		1 cm × 2 cm	0.12	88.91	This study

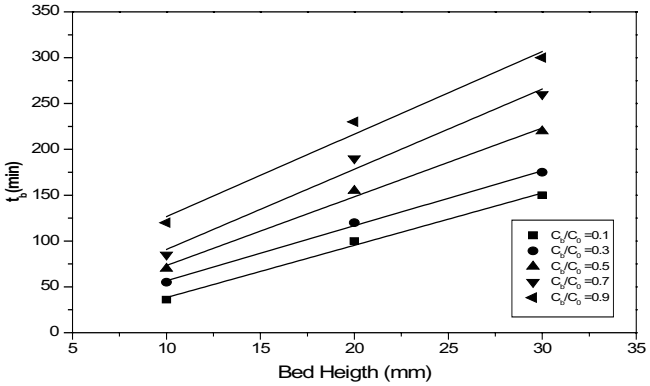

Fig. 15. Linear regression of BDST model at different breakthrough points (C_0 = 10 mg L^{-1} and F = 2 mL L^{-1}).

To understand better the adsorptive proprieties of ESM, the material was fully characterized using different methods. ESM is rich with amides, amines and carboxylic groups and exhibits a porous and interlaced fibrous morphology. The specific surface area was 13.38 m^2 g^{-1}. pH_{pzc} of ESM was found to be 7.51. Several operating parameters were investigated. Overall, the best adsorption capacity was found to be 41.49 mg g^{-1} under the following conditions: flow rate of 2 mL min^{-1}, Cr(VI) concentration of 5 mg L^{-1}, bed height of 20 mm, pH 3 and a temperature of 298 K.

The five models applied, Thomas, Yoon–Nelson, Bohart–Adams, Wolborska, and BDST were considered appropriate to describe the dynamic behavior for Cr(VI) adsorption.

Symbols

C_0 — Initial Cr(VI) concentration, mg L^{-1}
C_t — Effluent Cr(VI) concentration, mg L^{-1}
V_{eff} — Effluent volume, mL
F — Influent flow rate, mL min^{-1}
t_e — Time of exhaustion, min
t_b — Time at breakthrough, min
q_{total} — Total weight of Cr(VI) adsorbed by adsorbent in column, mg
q_{exp} — Weight of Cr(VI) adsorbed per g of adsorbent from experiment, mg g^{-1}
m — Adsorbent mass, g
N_{exp} — Experimental maximum sorption capacity, mg L^{-1}
V — Volume of solution, mL
R — Percentage of removal, %
W_{total} — Total amount of Cr(VI) sent to column, mg
C_{ads} — Adsorbed Cr(VI) concentration, mg L^{-1}
t — Service time of the column, min
K_{th} — Kinetic constant of Thomas model, L mg^{-1} min^{-1}
U — Linear velocity, mm min^{-1}
K_{YN} — Kinetic constant of Yoon–Nelson model, min^{-1}
K_{BA} — Kinetic constant of Bohart–Adams model, L mg^{-1} min^{-1}
Z — Height of the bed, mm
N_0 — Maximum sorption capacity, mg L^{-1}
C_b — Breakthrough concentration, mg L^{-1}
N'_0 — Adsorption capacity in BDST model, mg L^{-1}
T — Temperature, °C, K
pH_{pzc} — pH of point of zero charge
pH_i — Initial pH of the solution
pH_f — Final pH of the solution
ΔpH — Difference between pH_f and pH_i

Greek

τ — Time required for 50% adsorbate breakthrough from Yoon–Nelson model, min

β_a — Kinetic coefficient of the external mass transfer in the Wolborska model, min^{-1}

Acknowledgment

The authors would like to acknowledge the financial support of the Algerian Ministry of Higher Education.

References

[1] P.K. Tyagi, Study of potentiality of coal fly ash for the removal of Cr(VI) from industrial wastewater: equilibrium and kinetic studies, Int. J. Eng. Technol. Sci. Res., 4 (2017) 836–843.
[2] M. Costa, C.B. Klein, Toxicity and carcinogenicity of chromium compounds in humans, Crit. Rev. Toxicol., 3 (2006) 155–163.
[3] M.H. Dehghani, M.M. Taher, A.K. Bajpai, B. Heibati, I. Tyagi, M. Asif, S. Agarwal, V.K. Gupta, Removal of noxious Cr(VI) ions using single-walled carbon nanotubes and multi-walled carbon nanotubes, Chem. Eng. J., 279 (2015) 344–352.
[4] S.C.W. Sakti, Y. Narita, T. Sasaki, N.S. Tanaka, A novel pyridinium functionalized magnetic chitosan with pH-independent and rapid adsorption kinetics for magnetic separation of Cr(VI), J. Environ. Chem. Eng., 3 (2015) 1953–1961.
[5] R. Djellabi, F.M. Ghorab, S. Nouacer, A. Smara, O. Khireddine, Cr(VI) photocatalytic reduction under sunlight followed by Cr(III) extraction from TiO_2 surface, Mater. Lett., 176 (2016) 106–109.
[6] M. Moradi, A. Dehpahlavan, R. Rezaei Kalantary, A. Ameri, M. Farzadkia, H. Izanloo, Application of modified bentonite using sulfuric acid for the removal of hexavalent chromium from aqueous solutions, Environ. Health Eng. Manage., 2 (2015) 99–106.
[7] S.M. Borghe-ei, J. Goodarzi, M. Mohseni, A. Amouei, Efficiency of removing chromium from plating industry wastewater using the electrocoagulation method, Q. Int. Arch. Health Sci., 2 (2015) 83–87.
[8] R. Djellabi, B. Yang, Y. Wang, X. Cui, X. Zhao, Carbonaceous biomass-titania composites with Ti–O–C bonding bridge for efficient photocatalytic reduction of Cr(VI) under narrow visible light, Chem. Eng. J., 366 (2019) 172–180.
[9] F. Fu, Q. Wang, Removal of heavy metal ions from wastewaters: a review, J. Environ. Manage., 92 (2011) 407–418.
[10] M.B. Ahmed, J.L. Zhou, H.H. Ngo, W. Guo, N.S. Thomaidis, J. Xu, Progress in the biological and chemical treatment technologies for emerging contaminant removal from wastewater: a critical review, J. Hazard. Mater., 323 (2017) 274–298.
[11] S. Yadav, V. Srivastava, S. Banerjee, C.H. Weng, Y.C. Sharma, Adsorption characteristics of modified sand for the removal of hexavalent chromium ions from aqueous solutions: Kinetic, thermodynamic and equilibrium studies, Catena., 100 (2013) 120–127.
[12] S. Rangabhashiyam, N. Selvaraju, B.R. Mohan, P.K.M. Anzil, K.D. Amith, E.R. Ushakumary, Hydrous cerium oxide nanoparticles impregnated *Enteromorpha* sp. for the removal of hexavalent chromium from aqueous solutions, J. Environ. Eng., 142 (2016) 1–9.
[13] M.M. Matlock, B.S. Howerton, D.A. Atwood, Chemical precipitation of heavy metals from acid mine drainage, Water Res., 36 (2002) 4757–4764.
[14] X. Li, P.G. Green, C. Seidel, C. Gorman, J.L. Darby, Chromium removal from strong base anion exchange waste brines, J. AWWA, 108 (2016) E247–E255.
[15] P.A. Vinodhini, P.N. Sudha, Removal of heavy metal chromium from tannery effluent using ultrafiltration membrane, Text. Clothing Sustainable, 2 (2017) 5.
[16] R. Djellabi, M.F. Ghorab, T. Sehili, Simultaneous removal of methylene blue and hexavalent chromium from water using TiO_2/Fe(III)/H_2O_2/Sunlight, CLEAN – Soil, Air, Water, 45 (2017) 1–7.
[17] C. Djelloul, O. Hamdaoui, Removal of cationic dye from aqueous solution using melon peel as nonconventional low-cost sorbent, Desal. Wat. Treat., 52 (2014) 7701–7710.
[18] A. Bhatnagar, V.J.P. Vilar, C.M.S. Botelho, R.A.R. Boaventura, Coconut-based biosorbents for water treatment-A review of the recent literature, Adv. Colloid Interface Sci., 160 (2010) 1–15.
[19] D.S.I.V.M. Macoveanu, Ligno-cellulosic materials for wastewater treatment, Environ. Eng. Manage. J., 5 (2006) 119–134.
[20] D. Suteu, C. Zaharia, Sawdust as biosorbent for removal of dyes from wastewaters. Kinetic and thermodynamic study, Chem. Bull. "Politechnica" Univ., 56 (2011) 85–88.
[21] A. Bhatnagar, A.K. Jain, A comparative adsorption study with different industrial wastes as adsorbents for the removal of cationic dyes from water, J. Colloid Interface Sci., 281 (2005) 49–55.
[22] G. Crini, Non-conventional low-cost adsorbents for dye removal: a review, Bioresour. Technol., 97 (2006) 1061–1085.
[23] V. Nandini, P.T. Shruthi, S. Tharannum, V.K. Murthy, Study of eggshell membrane as a potent adsorbent of chromium, Int. J. Res., 2 (2015) 1262–1269.
[24] H. Daraei, A. Mittal, J. Mittal, H. Kamali, Optimization of Cr(VI) removal onto biosorbent eggshell membrane: experimental and theoretical approaches, Desal. Wat. Treat., 52 (2014) 1307–1315.
[25] B. Liu, Y. Huang, Polyethyleneimine modified eggshell membrane as a novel biosorbent for adsorption and detoxification of Cr(VI) from water, J. Mater. Chem., 43 (2011) 17413–17418.
[26] V. Ponnusami, V. Gunasekar, S.N. Srivastava, Kinetics of methylene blue removal from aqueous solution using gulmohar (*Delonix regia*) plant leaf powder: multivariate regression analysis, J. Hazard. Mater., 169 (2009) 119–127.
[27] J. Zhang, L. Chen, H. Yin, S. Jin, F. Liu, H. Chen, Mechanism study of humic acid functional groups for Cr(VI) retention: two-dimensional FTIR and 13C CP/MAS NMR correlation spectroscopic analysis, Environ. Pollut., 225 (2017) 86–92.
[28] A. Gupta, C. Balomajumder, Simultaneous continuous removal of Cr(VI) and phenol from binary synthetic simulated waste water in tea waste packed bed column: kinetic modeling, J. Dispersion Sci. Technol., 37 (2016) 656–664.
[29] H.C. Thomas, Heterogeneous ion exchange in a flowing system, J. Am. Chem. Soc., 66 (1944) 1664–1666.
[30] Y.H. Yoon, J.H. Nelson, Application of gas adsorption kinetics I. A theoretical model for respirator cartridge service life, Am. Ind. Hyg. Assoc. J., 45 (1984) 509–516.
[31] G.S. Bohart, E.Q. Adams, Some aspects of the behavior of charcoal with respect to chlorine, J. Am. Chem. Soc., 42 (1920) 523–544.
[32] A. Wolborska, Adsorption on activated carbon of p-nitrophenol from aqueous solution, Water Res., 23 (1989) 85–91.
[33] E.A. El-Sofany, R.E. Hassan, E.H. Borai, Fixed Bed Column Study for Separation of Light Lanthanides by Dowex-50X8, Environ. Eng. Sci., 2 (2011) 101–116.
[34] N. Wang, Z. Ma, S. Zhou, G. Liang, Facile fabrication of SERS substrate based on food residue eggshell membrane, Chem. Phys. Lett., 666 (2016) 45–50.
[35] J. Choi, B. Pant, C. Lee, M. Park, S.J. Park, H.Y. Kim, Preparation and characterization of eggshell membrane/PVA hydrogel via electron beam irradiation technique, J. Ind. Eng. Chem., 47 (2017) 41–45.
[36] W. Bessashia, Z. Hattab, Y. Berredjem, R. Djellabi, R. Zerdoum, A. Allaoui, A. Gheid, K. Guerfi, Utilization of powdered eggshell waste for rhodamine B removal: evaluation of adsorptive efficiencies and modeling studies, Sens. Lett., 16 (2018) 128–136.
[37] A. Mittal, M. Teotia, R.K. Soni, J. Mittal, Applications of egg shell and egg shell membrane as adsorbents: a review, J. Mol. Liq., 223 (2016) 376–387.
[38] B.D. Zdravkov, J.J. Čermák, M. Šefara, J. Janků, Pore classification in the characterization of porous materials: a perspective, Cent. Eur. J. Chem., 5 (2007) 385–395.
[39] S. Park, K.S. Choi, D. Lee, D. Kim, K.T. Lim, K.H. Lee, H. Seonwoo, J. Kim, Eggshell membrane: review and impact on engineering, Biosyst. Eng., 151 (2016) 446–463.
[40] B.J. Tiimob, G. Mwinyelle, W. Abdela, T. Samuel, S. Jeelani, V.K. Rangari, Nanoengineered eggshell-silver tailored copolyester

polymer blend film with antimicrobial properties, J. Agric. Food Chem., 65 (2017) 1967–1976.
[41] Z. Aksu, F. Gönen, Biosorption of phenol by immobilized activated sludge in a continuous packed bed: prediction of breakthrough curves, Process Biochem., 39 (2004) 599–613.
[42] O. Hamdaoui, Dynamic sorption of methylene blue by cedar sawdust and crushed brick in fixed bed columns, J. Hazard. Mater., 138 (2006) 293–303.
[43] Y. Yan, Q. An, Z. Xiao, W. Zheng, S. Zhai, Flexible core-shell/bead-like alginate@PEI with exceptional adsorption capacity, recycling performance toward batch and column sorption of Cr(VI), Chem. Eng. J., 313 (2017) 475–486.
[44] S. Sadaf, H.N. Bhatti, Batch and fixed bed column studies for the removal of Indosol Yellow BG dye by peanut husk, J. Taiwan Inst. Chem. Eng., 45 (2014) 541–553.
[45] M. Tamez Uddin, M. Rukanuzzaman, M. Maksudur Rahman Khan, M. Akhtarul Islam, Adsorption of methylene blue from aqueous solution by jackfruit (*Artocarpus heteropyllus*) leaf powder: a fixed-bed column study, J. Environ. Manage., 90 (2009) 3443–3450.
[46] R. Mazouz, N. Filali, Z. Hattab, K. Guerfi, Valorization of granulated slag of Arcelor-Mittal (Algeria) in cationic dye adsorption from aqueous solution: column studies, J. Water Reuse Desal., 6 (2016) 204–213.
[47] T. Zang, Z. Cheng, L. Lu, Y. Jin, X. Xu, W. Ding, J. Qu, Removal of Cr(VI) by modified and immobilized *Auricularia auricula* spent substrate in a fixed-bed column, Ecol. Eng., 99 (2017) 358–365.
[48] J. Pradhan, S.N. Das, R.S. Thakur, Adsorption of hexavalent chromium from aqueous solution by using activated red mud, J. Colloid Interface Sci., 217 (1999) 137–141.
[49] S.S. Baral, S.N. Das, P. Rath, Hexavalent chromium removal from aqueous solution by adsorption on treated sawdust, Biochem. Eng. J., 31 (2006) 216–222.
[50] F. Momenbeik, F.T. Riahi, Chemically modified eggshell membrane as an adsorbent for solid-phase-extraction of morphine followed by high performance liquid chromatography analysis, Anal. Bioanal. Chem. Res., 1 (2014) 108–116.
[51] Z. Zou, Y. Tang, C. Jiang, J. Zhang, Efficient adsorption of Cr(VI) on sunflower seed hull derived porous carbon, J. Environ. Chem. Eng., 3 (2015) 898–905.
[52] H. Wang, X. Yuan, Y. Wu, X. Chen, L. Leng, H. Wang, H. Li, G. Zeng, Facile synthesis of polypyrrole decorated reduced graphene oxide-Fe_3O_4 magnetic composites and its application for the Cr(VI) removal, Chem. Eng. J., 262 (2015) 597–606.
[53] M. Meng, Y. Feng, M. Zhang, Y. Liu, Y. Ji, J. Wang, Y. Wu, Y. Yan, Highly efficient adsorption of salicylic acid from aqueous solution by wollastonite-based imprinted adsorbent: a fixed-bed column study, Chem. Eng. J., 225 (2013) 331–339.
[54] R. Zerdoum, Z. Hattab, Y. Berredjem, R. Mazouz, Removal of methylene blue from water using eggshell membrane fixed bed, Desal. Wat. Treat., 81 (2017) 252–264.
[55] A. Singh, D. Kumar, J.P. Gaur, Continuous metal removal from solution and industrial effluents using *Spirogyra* biomass-packed column reactor, Water Res., 46 (2011) 779–788.
[56] Z.Z. Chowdhury, S.M. Zain, A.K. Rashid, R.F. Rafique, K. Khalid, Breakthrough curve analysis for column dynamics sorption of Mn(II) ions from wastewater by using *Mangostana garcinia* peel-based granular-activated carbon, J. Chem., 2013 (2013), doi: 10.1155/2013/959761.
[57] W. Zhang, L. Dong, H. Yan, H. Li, Z. Jiang, X. Kan, H. Yang, A. Li, R. Cheng, Removal of methylene blue from aqueous solutions by straw based adsorbent in a fixed-bed column, Chem. Eng. J., 173 (2011) 429–436.